iScience

CellPress
OPEN ACCESS

Article

Different explanations for surface and canopy urban heat island effects in relation to background climate

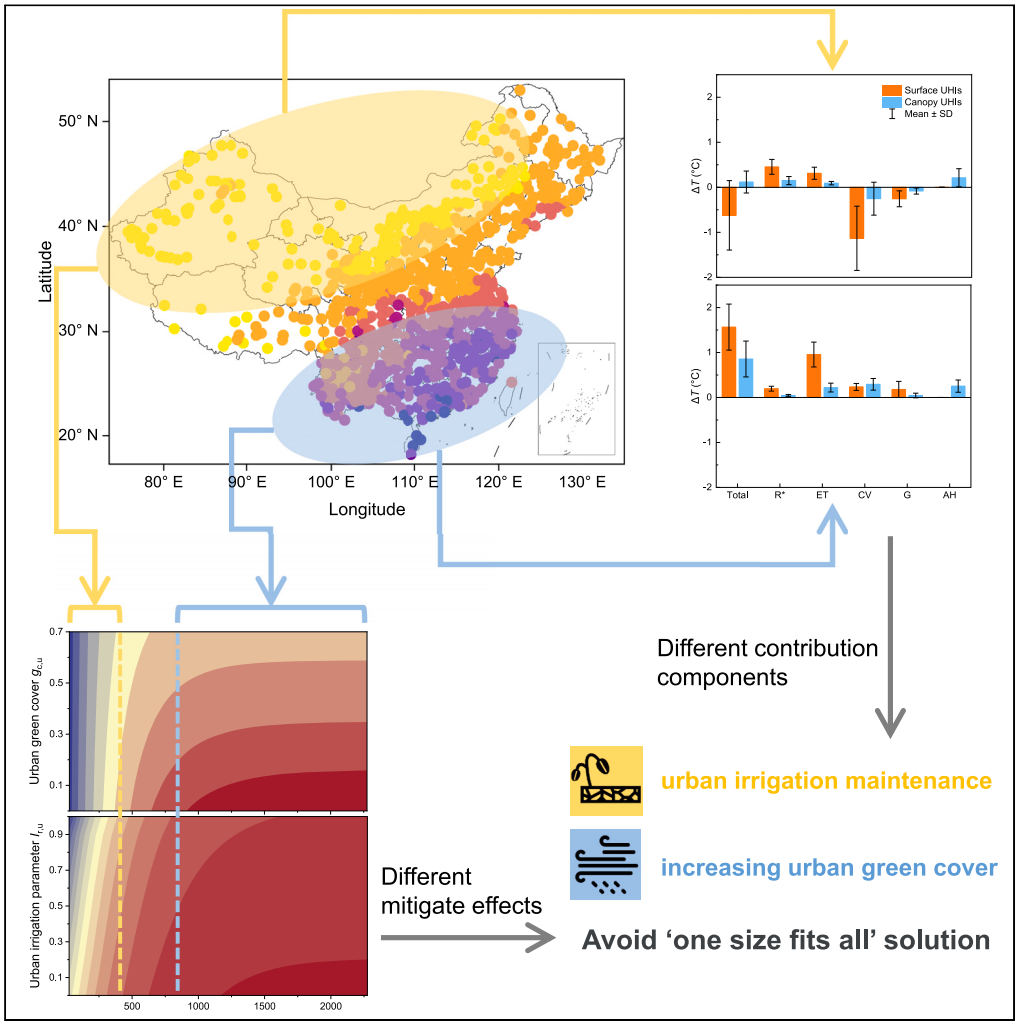

Liu Yang, Qi Li, Qiong Li, Lei Zhao, Zhiwen Luo, Yan Liu

liuyan@xauat.edu.cn

Highlights

Attribution models for SUHIs and CUHIs were developed

SUHIs and CUHIs show similar dependencies on background climate and urban morphology

Prioritize maintaining low building density, especially for mitigating CUHIs

Urban irrigation is more effective than urban greening in arid regions

Yang et al., iScience 27, 108863
March 15, 2024
https://doi.org/10.1016/j.isci.2024.108863

iScience

CellPress
OPEN ACCESS

Article

Different explanations for surface and canopy urban heat island effects in relation to background climate

Liu Yang,[1,5] Qi Li,[1,2,5] Qiong Li,[2] Lei Zhao,[3] Zhiwen Luo,[4] and Yan Liu[1,6,*]

SUMMARY

The background climatic conditions and urban morphology greatly influence urban heat island effects (UHIs), but one-size-fits-all solutions are frequently employed to mitigate UHIs. Here, attribution models for surface UHIs (SUHIs) and canopy UHIs (CUHIs) were developed to describe UHI formation. The contribution of factors to SUHIs and CUHIs shows similar dependencies on background climate and urban morphology. Furthermore, the factors that mainly contributed to CUHIs were more complex, and anthropogenic heat was the more critical factor. Influence from urban morphology also highlights that there is no one-size-fit-all solution for heat mitigation at the neighborhood. In particular, maintaining a low building density should be prioritized, especially mitigating CUHIs. Moreover, it is more effective to prioritize urban irrigation maintenance over increasing green cover in arid regions but the opposite in humid regions. The work can provide scientific evidence to support developing general and regional guidelines for urban heat mitigation.

INTRODUCTION

Urban development changes the energy balance in peri-urban areas, which typically have higher air and surface temperatures than their surrounding rural areas.[1,2] These well-known urban heat island effects (UHIs) can significantly affect the local climate[1] and aggravate heat stress,[3–5] with negative impacts on energy consumption[6,7] and air pollution.[8–10] UHIs are also a threat to human health, and a warming environment will increase the risk of morbidity and mortality,[3,11] especially when synergistic interactions with heat waves occur.[12,13] According to the *World Cities Report 2022: Envisaging the Future of Cities* by UN-Habitat, China's urban population is expected to exceed 1 billion by 2035, with an estimated increase of 180 million compared with 2020.[14] China's rapid urbanization will exacerbate the thermal risks faced by urban populations.[15,16] However, one-size-fits-all solutions are frequently employed to mitigate UHIs; another tendency is the conflation between the mitigation strategies of surface UHIs (SUHIs) and canopy UHIs (CUHIs). For instance, shading has a more pronounced cooling effect on surface temperatures than on air temperatures. Therefore, understanding the mechanisms responsible for the UHIs is important for identifying general guidelines to mitigate problems related to heat.

Howard observed higher air temperatures in London compared with surrounding rural areas to first identify the UHIs[17] and correctly hypothesized most of the causes that are now considered responsible.[1] However, selecting representative measurement sites for studies of the CUHIs is still a problem that needs to be addressed.[18,19] Due to the proliferation of satellite observations in the land surface temperature (LST) field, several studies have attempted to explain the mechanisms responsible for SUHIs.[20,21] The same sensor used in a single satellite can provide complete global coverage observation data to obtain large-scale surface temperature observations for applications in comparative studies of cities under different background climatic conditions. However, considering that most vertically oriented building faces are not observed by a nadir-viewing remote imaging radiometer, satellite-based LST data cannot fully represent all of the urban surface temperatures in areas with complex three-dimensional geometry.[22,23] In recent studies, the attribution analysis method was applied at city scale to show that the urban–rural contrast in evapotranspiration (*ET*) and/or thermal convection efficiency are the main determinants of summer SUHIs,[24,25] and the background climatic conditions affect the relative contributions of these factors.[2] On a relatively long-period, SUHIs exhibit a tightly connection with CUHIs, with large SUHIs will experience a large CUHIs.[26] However, observational studies have shown that SUHIs and CUHIs differ in terms of their frequency and characteristics.[27,28] Some similar biophysical drivers affect the development of SUHIs and CUHIs, but they may differ in terms of magnitude.[21] Therefore, the quantitative study on SUHIs in the previous study does not provide a comprehensive

[1]State Key Laboratory of Green Building, Department of Architecture, Xi'an University of Architecture and Technology, Xi'an, Shaanxi 710055, P.R. China
[2]State Key Laboratory of Subtropical Building and Urban Science, School of Architecture, South China University of Technology, Guangzhou 510640, P.R. China
[3]Department of Civil and Environmental Engineering, University of Illinois at Urbana-Champaign, Urbana, IL, USA
[4]Welsh School of Architecture, Cardiff University, Cardiff, UK
[5]These authors contributed equally
[6]Lead contact
*Correspondence: liuyan@xauat.edu.cn
https://doi.org/10.1016/j.isci.2024.108863

understanding of CUHIs; the quantitative attribution of CUHIs remains unclear. Unfortunately, these attribution analysis studies mainly focused on the SUHIs and relatively few have considered the CUHIs.[29] In particular, compared with the SUHIs, the CUHIs is more relevant to outdoor thermal health[30] because heat stress is a function of air temperature and not necessarily LST.[31,32] Thus, it is important to understand the mechanisms responsible for CUHIs.

In the present study, we focused on urban residential areas where the human activity is more intense. Based on the first-order Taylor series expansion of a linearized energy balance equation, we developed a mechanistic attribution model for linking ΔT to net radiation (R^*), evapotranspiration (ET), convection efficiency (CV), heat storage (G), and anthropogenic heat (AH), which used to determine the key factors. This model is based on the fact that during the development of a city, the urban underlying surface changes and coupled with increases in human activity and energy consumption, will lead to change in the original energy balance of this area, and this is considered the main cause of the UHIs. Therefore, background climatic conditions and urban morphology combine to impact the formation of the UHIs. Then, we apply this mechanistic attribution model to discuss the individual and combined effects of background climatic conditions and urban morphology on the formation of SUHIs and CUHIs. The differences in impacts of heat mitigation strategies on SUHIs and CUHIs under different background climatic conditions and their influence by urban morphology were also compared, to provide support for developing general guidelines for urban heat mitigation.

RESULTS

Attribution of UHIs

Figures 1A and 1B show the attributions to the summer SUHIs and CUHIs intensities for 990 cities across China. Clearly, the main contributors to the summer SUHIs and CUHIs intensities are the urban–rural differences in the evapotranspiration (ΔET) and convection efficiency (ΔCV). In particular, when with a low urban irrigation index ($I_{r,u} = 0$), the largest contributor to the SUHI intensities was ΔET, which is consistent with the findings obtained by Li et al.,[24] and it can be explained by the lower soil moisture and vegetation in urban areas. However, the contribution of ΔET was significantly reduced when the idealized urban irrigation index ($I_{r,u} = 1$) was adopted. Higher $I_{r,u}$ will make the evapotranspiration from vegetation in urban areas not be limited by the soil moisture, even with the lower green cover in urban areas, resulting in negative contribution of ΔET, which is more obvious in arid regions. In fact, ΔET also exhibits a large standard deviation (SD), and it is considered that the differences in heat mitigation achieved by urban irrigation are great under different background climatic conditions. Unlike the SUHIs, the difference in the contributions of ΔET and ΔCV to the CUHI intensities was not significant. In the present study, the convection efficiency included the convective heat exchange between the canopy air and urban underlying surface, and the convective heat exchange between the canopy air and underlying atmosphere, which is more pronounced for a fluid such as air due to flow. Given the impact of the geometric configuration of an urban canyon on radiation exchanges, the urban canyon receives more net radiation (R^*) than rural areas,[33] and the contribution of ΔR^* is positive. It is important to note that the difference between urban and rural areas is small, so the contribution of the net radiation is not significant. Meanwhile, the heat stored (G) during the daytime was released at nighttime, and the value of G was close to 0 when time scales exceed a day, i.e., the contribution of ΔG was also small. In addition, the contributions of both ΔR^* and ΔG to the SUHI intensities were slightly higher than those to the CUHI intensities. It is considered that if the heat stored in air is ignored, $R^*$and G have direct effects on the urban surfaces and an indirect effect on the urban canopy air, and thus the effect on the CUHI intensities is weaker.

According to the mean annual precipitation (P), cities in arid regions ($P < 400$ mm yr^{-1}) and humid regions ($P \geq 800$ mm yr^{-1}) were selected to analyze the contributions to the summer SUHI intensities and summer CUHI intensities (see Figures 1C–1F). ΔT_s ranged from −2.9°C to −0.4°C in arid regions (mean: −0.6°C), and from 0.1°C to 3.2°C in humid regions (mean: 0.9°C). The ΔT_s values were much smaller for cities in arid regions than humid regions, and the specific contributions to ΔT_s also differed significantly between arid and humid regions. The average contribution of ΔR^* was 0.5°C in arid regions, which was higher than the contribution in humid regions (0.2°C), mainly because the solar radiation is generally higher in arid regions (see Figure S1B). The contributions of ΔET and ΔCV were very different in arid and humid regions, and the contribution of ΔCV was much higher than that of ΔET in arid regions. Given the short vegetation found in arid regions, cities are generally aerodynamically rougher than the surrounding rural areas and the heat dissipation by convection could be more efficient,[34] and thus ΔCV made a negative contribution to ΔT_s. Urban areas had lower vegetation cover in arid regions, and water limitations reduced the ET by vegetation in arid rural areas, thereby limiting the contribution of ΔET to ΔT_s. However, the largest contributor to ΔT_s was ΔET in urban areas where higher precipitation resulted in a higher soil water content, thereby reducing the restriction on ET by vegetation, and the lower vegetation cover in urban areas led to higher ΔET values, and the contribution to ΔT_s was positive. Cities in humid regions are generally surrounded by tall vegetation, and there was no significant difference in heat dissipation by convection between urban and rural areas, thereby reducing the contribution of ΔCV to ΔT_s. The contributions to ΔT_c were similar to those to ΔT_s, but the differences in the contribution of each factor to ΔT_c were much smaller compared with ΔT_s. In addition, ΔCV provided similar contributions to ΔT_s and ΔT_c in humid regions, with values of 0.2°C and 0.3°C under $I_{r,u} = 0$ (0.2°C and 0.2°C under $I_{r,u} = 1$), respectively. Whereas, ΔCV provided a significantly greater contribution to ΔT_s than ΔT_c in arid regions, with values of −1.1°C and −0.3°C under $I_{r,u} = 0$ and −1.0°C and −0.2°C under $I_{r,u} = 1$, respectively. The contribution of anthropogenic heat (AH) was high in both arid and humid regions. Consistent with previous studies, the thermal mitigation effect achieved by increasing the urban irrigation index was influenced by the background climatic conditions.[26,35] Increasing the urban irrigation index reduced the contribution of ΔET to ΔT_s from 0.3°C to −1.6°C in arid regions, but only from 1°C to 0.4°C in humid regions. In addition, the effect of this measure on ΔT_c was relatively weak, where the contribution of ΔET only decreased from 0.1°C to −0.5°C in arid regions.

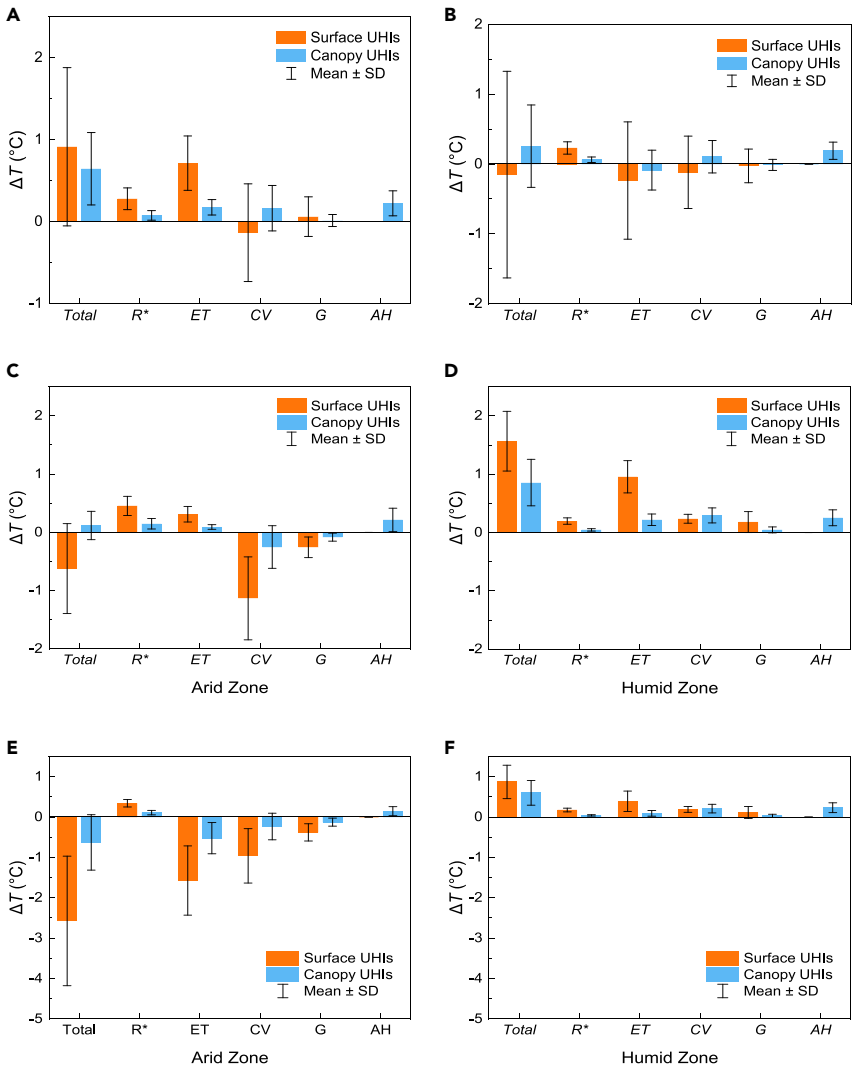

Figure 1. Attributions of summer surface and canopy urban heat islands (UHIs) across China

(A and B) Summer UHIs (surface UHIs, orange; canopy UHIs, blue) and components considering urban irrigation indexes of (A) $I_{r,u}$ = 0 and (B) $I_{r,u}$ = 1.

(C and D) Modeling results considering an urban irrigation index of $I_{r,u}$ = 0 in arid regions (C) and (D) humid regions.

(E and F) Modeling results considering an urban irrigation of index $I_{r,u}$ = 1 in (E) arid regions and (F) humid regions. The urban irrigation index is a coefficient describing the level of irrigation, establishing the connection between actual and potential evapotranspiration. For $I_{r,u}$ = 0, it describes the actual evapotranspiration under natural background climatic conditions. For $I_{r,u}$ = 1, it means there is no water supply limitation and that actual and potential evapotranspiration are equal. Error bars indicate ±1 standard deviation.

Influence of background climate

We quantified the contributions to ΔT from different biophysical factors comprising *R**, *ET*, *CV*, *G*, and *AH* (see STAR Methods). The distributions of the contributions to ΔT in China from different biophysical factors are shown in Figure 2. Without urban irrigation ($I_{r,u}$ = 0), the distribution of the contribution from ΔET to ΔT_s was similar to the distribution for mean annual precipitation in China (see Figure S2). In cities where $P < 400$ mm yr^{-1}, the contribution of ΔET was low and generally below 20%, and the contribution to ΔT_s was dominated by ΔCV with greater than −60%, where "–" implies an inverse effect on ΔT_s. ΔET made the dominant contribution to ΔT_s in humid regions, especially in cities where $P > 1200$ mm yr^{-1}, and the contribution of ΔET exceeded 90%. As I_{ru} increased, the contribution of *ET* also increased in arid regions, but with the reverse effect on ΔT_s, and this influence gradually expanded from northwest China (arid regions) to southeast China (humid regions). However, in southeast China, *ET* still made a high positive contribution to ΔT_s, especially in areas where $P > 1600$ mm yr^{-1}, and ΔET still contributed more than 80%, thereby implying that improving urban irrigation levels alone had a limited impact on mitigating UHIs. It was also found that under idealized urban irrigation ($I_{r,u}$ = 1), the contribution of ΔT_s was more complex in some cities where $800 < P < 1200$ mm yr^{-1}, and both ΔET and ΔCV did not make major contributors, and their contributions were similar. As mentioned earlier, the composition of

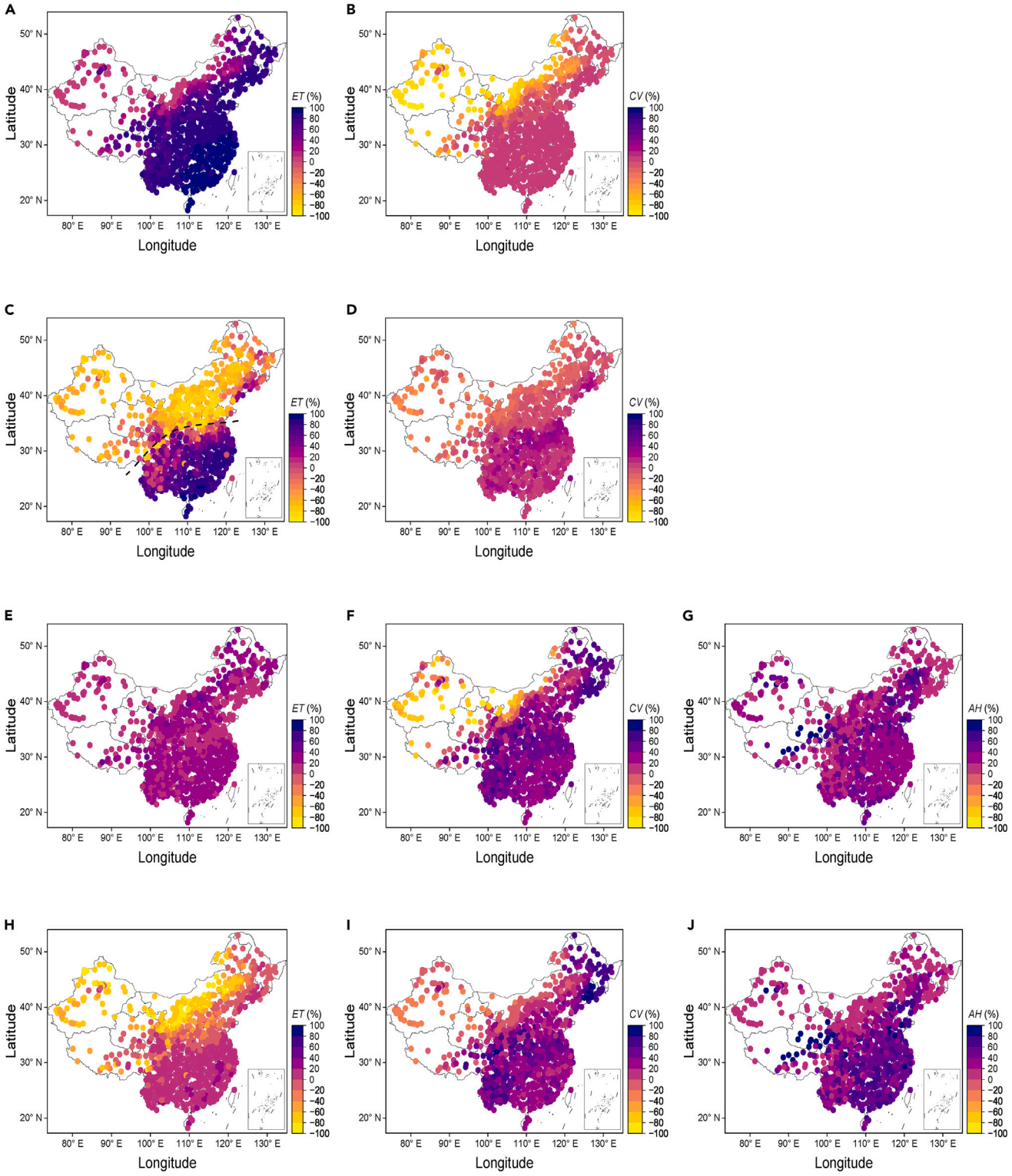

Figure 2. Distribution of the contribution of each component to summer surface and canopy urban heat islands (UHIs) under different urban irrigation indexes

(A–D) Surface UHIs and (E–J) canopy UHIs, [(A–B) and (E–G)] under urban irrigation index $I_{r,u}$ = 0 and [(C–D) and (H–J)] under urban irrigation index $I_{r,u}$ = 1.

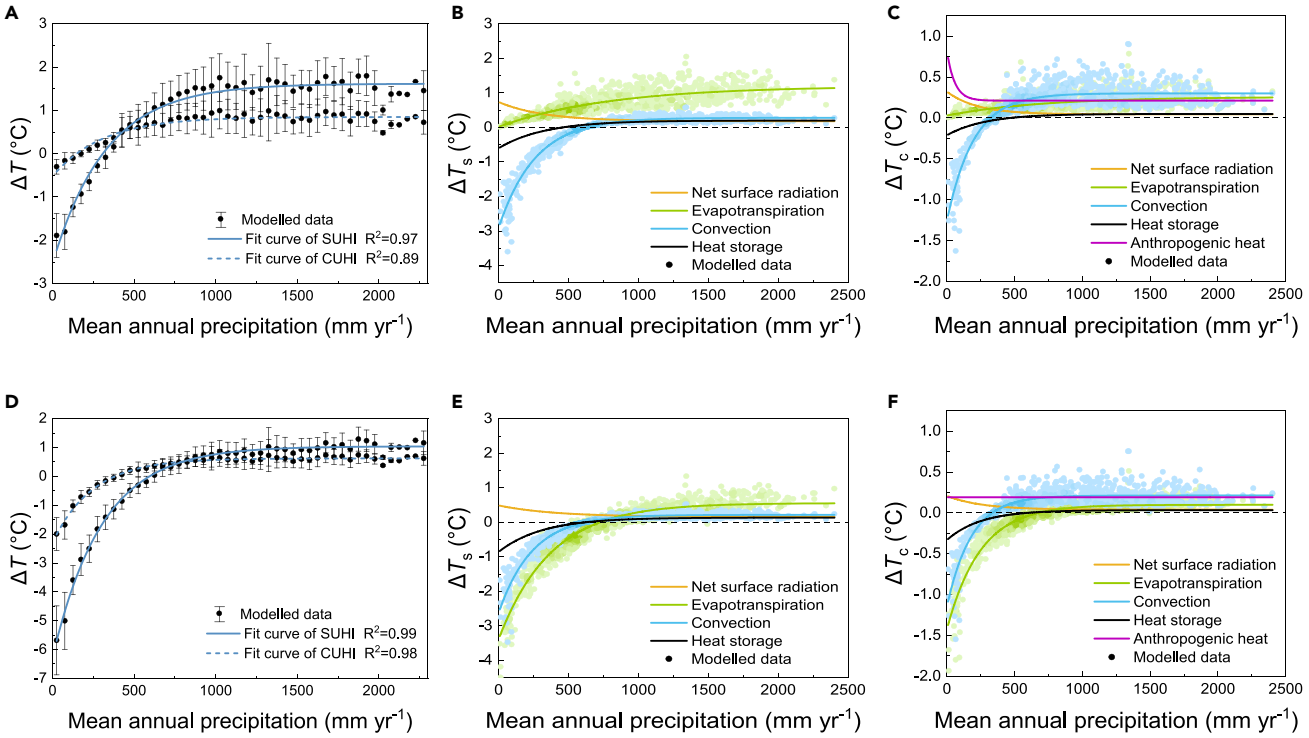

Figure 3. Effects of precipitation on summer surface and canopy urban heat island effects (UHIs) and components

(A–C) Urban irrigation index I_{ru} = 0. Modeled (markers) and fitted (lines) nonlinear relationships between ΔT (ΔT_s and ΔT_c) and (A) mean annual precipitation (P), (B) components of ΔT_s, and (C) components of ΔT_c.

(D–F) Urban irrigation index I_{ru} = 1. Modeled (markers) and fitted (lines) nonlinear relationships between ΔT (ΔT_s and ΔT_c) and (D) mean annual precipitation, (E) components of ΔT_s, and (F) components of ΔT_c. The line was obtained by fitting the mean values for the modeled data. Error bars indicate ±1 standard deviation.

the contributors to ΔT_c was more complex compared with ΔT_s, and it was difficult to identify the main contributors to ΔT_c, which also suggests that it may be more complex to mitigate ΔT_c compared with ΔT_s. The dominant contributor was more likely to be identified in arid regions (P < 400 mm yr^{-1}), where ΔCV and ΔET accounted for >60% of the inverse contributions under $I_{r,u}$ = 0 and $I_{r,u}$ = 1, respectively. Given the influence of latitude, the contribution of ΔAH was higher in cities at low latitudes than high latitudes during the summer.

A nonlinear relationship between ΔT (ΔT_s and ΔT_c) and mean annual precipitation was found (see Figure 3A), which is consistent with the results obtained on a global scale by Manoli et al.[2] However, compared with their findings, ΔT_s was slightly lower in the present study because cities in arid regions in China contain high buildings and urban areas have a stronger convective efficiency compared with suburban areas with short vegetation, as shown in Figure 3B. In low precipitation regions, ΔT_s increased in a linear manner with precipitation, and ΔT_s saturated at high precipitation values exceeding $P \approx$ 1,000 mm yr^{-1} ΔT_c shows a similar trend to ΔT_s but reached saturation at $P \approx$ 500 mm yr^{-1}. It was also found that the magnitude of the change in ΔT_s was much larger than that in ΔT_c, where the latter was influenced less by the background climatic conditions. The P–ΔT relationship was mainly controlled by ΔET and ΔCV, especially ΔCV, which had a similar shape to the P–ΔT relationship. In humid regions with high relative air humidity, the vapor pressure deficit in the air was low, thereby restricting the ET by vegetation in rural areas. Thus, an upper bound for ΔET was defined between urban and rural environments. Conversely, water limitations reduced the magnitude of ET in rural arid regions, thereby limiting the contribution of ΔET to ΔT (see Figures 3B and 3C). Considering the larger "deficit" of water in the air, supplementing the water budget of urban vegetation with irrigation increased the ET in urban areas, and it made a negative contribution to ΔT, thereby creating an "oasis" effect[36] (see Figures 3E and 3F). As discussed earlier, the height of natural vegetation increases with precipitation, and thus the heat dissipation efficiency by convection decreased in rural areas as the precipitation increased. Therefore, the urban–rural differences in the convection efficiency also contributed to cooling cities in arid regions.[24,25] By contrast, the tall vegetation that surrounded cities in humid regions exchanged heat more efficiently than dense building blocks, and ΔCV made a positive contribution to ΔT.

The ΔET–ΔT and ΔCV–ΔT relationships had similar shapes for ΔT_s and ΔT_c. According to Equation 6 and Equation 10, the energy redistribution factors f_s and f_c represent the sensitivities of ΔT_s and ΔT_c to energy forcing of 1 W m^{-2}. As shown in Figure S3, the energy redistribution factor f_c for ΔT_c was higher than f_s for ΔT_s, thereby damping the influence of urban–rural differences in energy forcing on the magnitude of ΔT_c. In addition, to calculate the contribution of ΔCV to ΔT_c, the convective heat exchange between the urban surface and canopy air was also considered, which generally had a positive influence. Therefore, this reduced the negative influence of ΔCV on ΔT_c in arid regions,

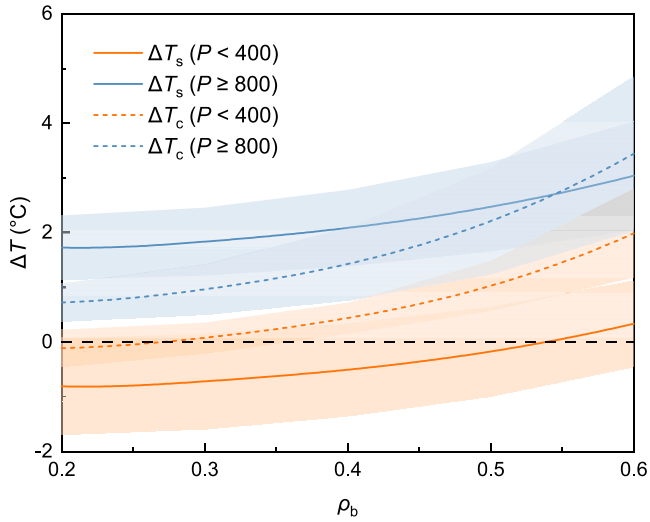

Figure 4. Effects of different building densities on the urban heat island effect in arid (orange) and humid regions (blue)
Solid lines (ΔT_s) and dashed lines (ΔT_c) indicate the ensemble means, and shaded areas represent the ensemble mean ±1 standard deviation.

whereas ΔCV had a greater positive influence on ΔT_c than ΔT_s in humid regions. It was also found that f_s and f_c varied with P, which tended to be higher in humid regions (see Figure S3). Thus, temperatures were more stable in humid areas and less susceptible to energy forcing, which may also explain the difficulty mitigating UHIs in these cities because it is necessary to eliminate more heat fluxes.

Influence of urban morphology

We selected a building density (ρ_b) range of 0.2–0.6 to analyze the influence of differences in urban morphology on the UHIs in arid and humid regions. In contrast to urban green cover, the influence of urban morphology on the UHIs was affected less by the background climatic conditions. In arid and humid regions, the ΔT–ρ_b relationship had a similar nonlinear shape, and ΔT_c was influenced more significantly by the building density compared with ΔT_s (see Figure 4). The attribution of UHI intensities for building densities of 0.2 and 0.6 were analyzed (see Figure 5). Under a building density of 0.2, ΔT_s was slightly higher than ΔT_c, whereas the opposite was found with the building density of 0.6. The dominant contributor to ΔT_s was ΔET in both the cases, and the different contribution of ΔET to ΔT_s was also influenced by background climatic conditions, which shows more significance in high precipitation regions (see Figure S7A). ΔET also shows a similar contribution trend to ΔT_c, but the contributions of ΔET, ΔCV, and ΔAH to ΔT_c were all around 0.15°C, with no significant dominant contributor (ρ_b = 0.2, see Figure 5A). The contribution of ΔCV to ΔT_s and ΔT_c still cannot be ignored and increases significantly with increasing building density, especially for ΔT_c. In contrast to ΔET, the different contribution of ΔCV to ΔT_s or ΔT_c is more significant in arid regions, whereas the contribution to ΔT_c is more susceptible to the influence of building density compared with ΔT_s (see Figure S7). It is suggested that as the building density increased, higher building densities restricted the efficiency of convective heat transfer from the urban surface and urban canopy to the atmosphere, thereby resulting in poorer heat dissipation with a negative impact on the UHIs. The higher building density also led to more anthropogenic heat[37,38] and when coupled with the poor heat dissipation, the contribution of ΔAH to ΔT_c was significant at a building density of 0.6 (see Figure 5B). Therefore, maintaining lower building densities is beneficial for urban heat mitigation, which provides greater heat dissipation and space for urban greening. It needs to be clarified that as the urban population is growing, choosing higher buildings or building densities to accommodate urban residents still requires further research, because the exact relation between aerodynamic resistance and urban morphology is complicated.[24] The urban morphology should be able to enhance heat dissipation performance.

Heat mitigation strategies

Urban greenery is used as a strategy for mitigating the UHIs, and it plays an important role in promoting the urban outdoor thermal environment as well as enhancing the thermal comfort of residents.[39,40] It shows that the $g_{c,u}$–ΔT relationship was strongly influenced by the background climatic conditions in urban areas (see Figures 6A and 6B). In humid regions, the ET by vegetation is less water limited, and it is a dominant component of the surface energy balance in rural areas.[41] The urban–rural ET difference was significant due to the lack of vegetation in cities, and thus increased vegetation cover is needed to reduce ΔT_s and ΔT_c. This means that it is difficult to reduce ΔT_s and ΔT_c by only focusing on vegetation strategies in higher precipitation regions (P > 1000 mm yr^{-1}), because the growth of vegetation is strongly dependent on the precipitation and humidity.[42] Indeed, to achieve ΔT_s < 1°C, almost the entire city area would need to be replaced with vegetation, and it is almost impossible to achieve ΔT_s < 0.5°C without urban irrigation management ($I_{r,u}$ = 0). The $g_{c,u}$–ΔT relationship had a similar shape for ΔT_s and ΔT_c, but with a lower value of ΔT_c, it is more feasible to achieve a weak ΔT_c by applying urban greenery strategies. In addition to increasing urban green cover, improving urban irrigation is an effective method for achieving urban cooling (see Figures 6C and 6D). In

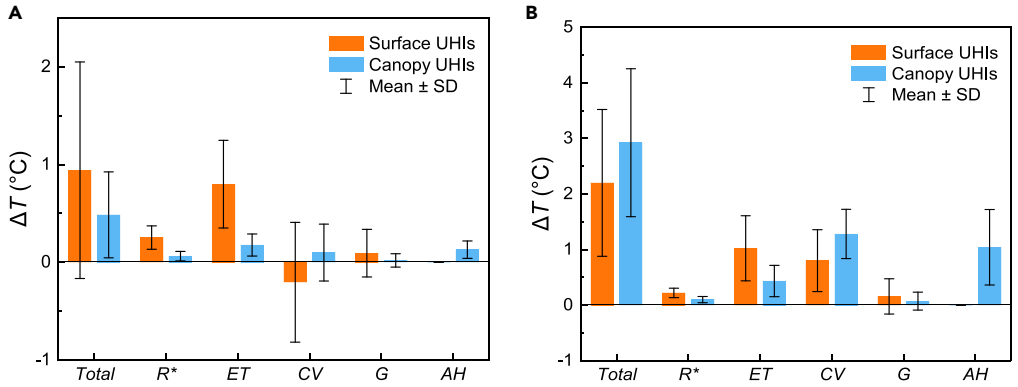

Figure 5. Attribution of summer surface and canopy urban heat island effects (UHIs) under different building densities

Summer UHIs (surface UHIs, orange; canopy UHIs, blue) and their components at: (A) building density ρ_b = 0.2 and (B) building density ρ_b = 0.6. Error bars indicate ±1 standard deviation.

particular, the low soil moisture content in arid regions will limit the evapotranspiration by rural vegetation to a certain extent.[2] Therefore, increasing urban irrigation can effectively increase the soil moisture content and reduce the limitation on vegetation evapotranspiration, achieving high heat mitigation even with low urban green cover ($g_{c,u}$ = 0.3). A recent study has shown that urban irrigation in more arid areas can improve the potential cooling performance.[43] By contrast, in humid regions with high soil moisture contents, the evapotranspiration by vegetation is less restricted by water, and thus the heat mitigation effect achieved by increasing urban irrigation is weaker (see Figure S10).

Clearly, increasing urban green cover and urban irrigation are both feasible strategies for mitigating the heat island effect.[44,45] In addition, according to further analysis, the effects achieved by these two measures also differed among different background climatic conditions. Urban green cover of 0 was set as a base case, and it was considered the UHI mitigation effect is achieved by increasing urban green cover under different urban irrigation indexes (see Figure S8). Under a low urban irrigation index ($I_{r,u}$ = 0.3), the heat island mitigation effect achieved by increasing urban green cover was more significant in humid regions, and this effect saturated at high precipitation values exceeding $P \approx 1000$ mm yr^{-1} (see Figure S8B). Interestingly, the UHI mitigation effect decreased with increasing precipitation in arid regions ($P < 400$ mm yr^{-1}). It is suggested that the difference between the potential evapotranspiration (*PET*) and mean annual precipitation decreased rapidly in this range ($P < 400$ mm yr^{-1}) (see Figure S9), and this difference indicates a contradiction between the positive effect of ambient air moisture deficit on vegetation evapotranspiration and the limitation imposed on vegetation evapotranspiration by the lack of available water. Therefore, the results suggested that urban irrigation management was more important in arid regions, even with a low urban irrigation index ($I_{r,u}$ = 0.3), where the water provided by irrigation could promote the evapotranspiration by vegetation, and the UHI mitigation effect decreased as the precipitation increased. By contrast, with no urban irrigation management ($I_{r,u}$ = 0), the evapotranspiration by vegetation was affected by the availability of water, and the situation mentioned earlier did not occur, and the UHI mitigation effect increased with the precipitation. In addition, significant differences in the heat island mitigation effects were found as the urban green cover increased in humid regions (see Figure S8A). The opposite situation occurred under a higher urban irrigation index ($I_{r,u}$ = 1), where the heat island mitigation effect of greater urban green cover increased in a nonlinear manner as the precipitation increased, before saturating at precipitation of $P \approx 500$ mm yr^{-1}, which is consistent with the results shown in Figure S9 to further illustrate the importance of urban irrigation management in arid regions (see Figure S10). The mitigation effect was much lower for ΔT_c than ΔT_s, i.e., about half of that for ΔT_s, and both exhibited similar trends. This can be explained by the higher energy redistribution factor of ΔT_c than ΔT_s.

The effectiveness of heat mitigation strategies is influenced not only by background climatic conditions but also by urban morphologies. The Mann-Whitney U test was used to analyze whether the heat mitigation with different building density had a significant difference, as shown in Figures S11A and S11B. The heat mitigation strategy obtains more significant effects at the higher building density ($p < 0.01$) and shows more difference in reducing ΔT_c than ΔT_s. At $I_{r,u}$ = 0.2, the reduction of ΔT_s and ΔT_c by increasing urban green cover from 0 to 0.4 was more significant in humid regions, even at a building density of 0.6 (see Figure S11C). It needs to be clarified that although the heat mitigation effect of increasing urban green cover is weaker at ρ_b = 0.2 than at ρ_b = 0.6, more space can be provided for urban greening at ρ_b = 0.2, which can further reduce ΔT_s and ΔT_c. In arid regions, increasing the urban irrigation index to reduce ΔT_s and ΔT_c was more favorable, and the urban morphology still shows a significant effect on reducing ΔT_c compared with ΔT_s (see Figure S11D). Fortunately, heat mitigation strategies can still have significant effects at higher building densities under different background climatic conditions, which of course requires a combination of urban greening and management of urban irrigation. It needs to be clarified that heat mitigation strategies will increase air humidity, especially in humid regions, which may further increase heat risk.[46]

DISCUSSION

In the UHI biophysical mechanism model, the difference between the urban and rural surface temperature (ΔT_s) and air temperature (ΔT_c) is attributed to different biophysical factors, thereby improving the understanding of the impacts of energy balance changes caused by

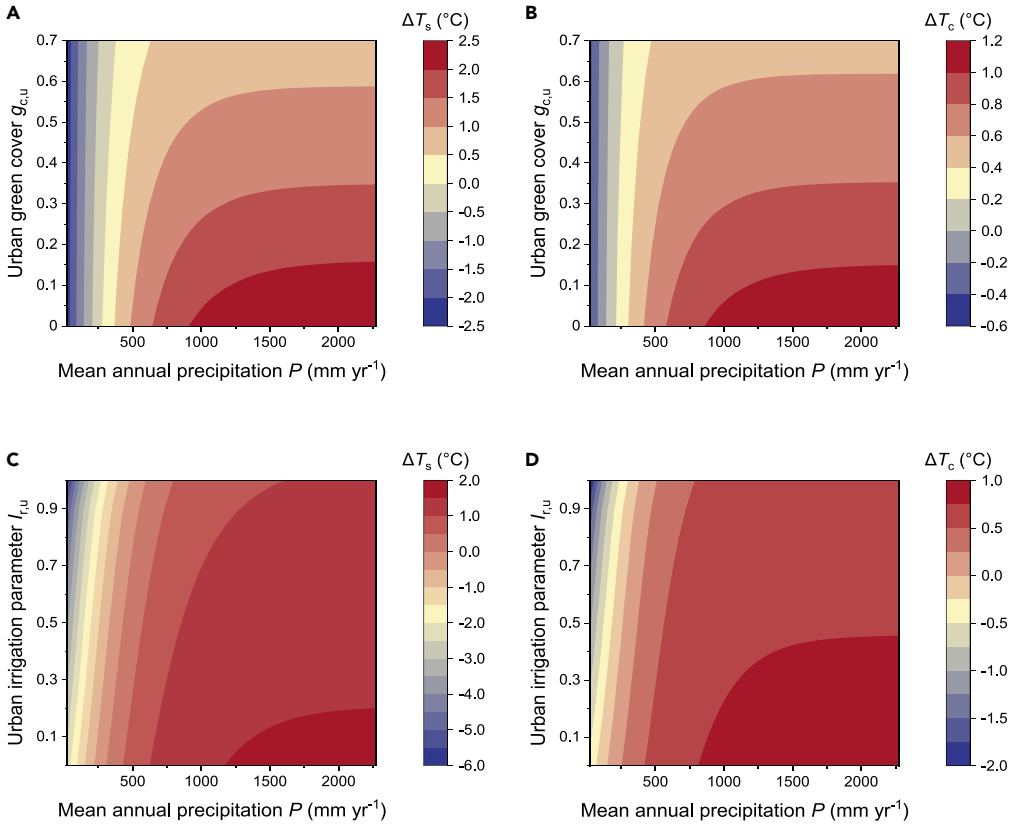

Figure 6. Impact of urban background climate on the efficiency of heat mitigation by urban evapotranspiration

(A and B) Mitigation effect of urban green cover change on (A) ΔT_s and (B) ΔT_c.

(C and D) Mitigation effect of urban irrigation changes on (C) ΔT_s and (D) ΔT_c. Results are shown for $I_{r,u}$ = 0.2 in (A–B) and for constant green cover $g_{c,u}$ = 0.3 in (C–D).

urbanization on the LST and air temperature. In the present study, it is demonstrated that the urban–rural differences in evapotranspiration (ΔET) and the convection efficiency (ΔCV) made the two main contributions to ΔT_s. Considering that anthropogenic heat release will directly cause air temperature increases, anthropogenic heat flux also had an important effect on ΔT_c, thereby making the mitigation of ΔT_c more complicated. It needs to be clarified that the air temperature rise due to anthropogenic heat release will also play an indirect effect on the surface temperature by limiting the release of heat from the urban surface. However, it has been shown to play a negligibly small role in contributing to ΔT_s^2, so we do not consider it as a factor affecting ΔT_s. Urban background climatic conditions significantly influenced the components that contributed to ΔT_s and ΔT_c, and the relationship between ΔT and mean annual precipitation was nonlinear.

Anthropogenic heat release will directly cause air temperature increases, which also had an important effect on ΔT_c, especially at the higher building density. Furthermore, the energy redistribution factor of ΔT_c (f_c) is generally higher than that of ΔT_s (f_s), which means it is necessary to eliminate more heat fluxes to reducing ΔT_c. Therefore, the factors that contribute to ΔT_c are more complex than ΔT_s, and it may be more challenging to mitigate ΔT_c. Maintaining a low building density should be prioritized, especially when mitigating ΔT_c, which can provide more space for urban greenery and further reduce anthropogenic heat emissions.

Increasing urban green cover is an important strategy for mitigating the UHIs,[44,47] and the effect of this strategy was influenced by the background climatic conditions.[35,47] Without urban irrigation, the effect of increasing urban green cover on mitigating UHIs was more pronounced in humid regions, but mitigation was difficult to achieve with a lower ΔT_s and ΔT_c. In arid regions, it is particularly important to improve urban irrigation considering the limitations imposed by soil water deficit on evapotranspiration. It is important for mitigating the UHIs, and a highly significant mitigation effect can be obtained by increasing urban irrigation even with low urban green cover. However, the irrigation strategy might jeopardize scarce water resources when considering the urban heat mitigation.[48] Meanwhile, urban greening and urban irrigation may lead to elevated humidity levels, which is also an important contributor to human heat stress.[46] Although urban greenery can effectively reduce ΔT_c, its mitigation effect was much lower than ΔT_s, about half of that for ΔT_s.

The contributions of urban–rural heat differences in the convection efficiency to ΔT_s and ΔT_c are more complicated to assess. Because the exact relation between aerodynamic resistance and urban morphology is complicated, it is difficult to artificially change the efficiency of urban convection. Generally, the positive impact of ΔCV on ΔT_c was higher than that on ΔT_s, at different building densities. Thus, improving urban

convective heat exchange efficiency plays more significant role in mitigating ΔT_c than mitigating ΔT_s, which means maintaining a low building density is most important for mitigating ΔT_c. Improving urban convective heat exchange efficiency may be more important in those cities with water limitations by changing the urban morphology.[21] Unfortunately, this heat mitigation strategy will face more challenges, as their exact relations are complicated.[24] This heat mitigation strategy was difficult to use in built-up neighborhoods where buildings already exist. For new neighborhoods, rational urban morphology design can be considered to improve urban convective heat exchange efficiency.

Limitations of the study

Generally, improving the urban evapotranspiration capacity and urban convective heat exchange efficiency plays an important role in mitigating ΔT_s and ΔT_c.[2,24] In arid regions, it is more important to improve urban irrigation than increasing the urban green cover. By contrast, in humid areas, it is quite important to maintain high urban green cover in urban areas to reduce the negative impacts of urban–rural differences in evapotranspiration on ΔT_s and ΔT_c considering the strong evapotranspiration capacity in rural areas.[2] However, the present model does not consider the effects of impervious surfaces on the urban water balance (the soil moisture may be lower in urban areas than suburban areas) but ensuring adequate urban irrigation is important. Urban morphology also affects the effectiveness of heat mitigation strategies. Targeted solutions should be proposed for different neighborhoods of the same city, especially in humid regions, where the impact of differences in urban morphology was more obvious. Furthermore, our discussion is limited to the summer-averaged SUHIs and CUHIs; some specific climatic conditions such as large-scale and local circulation, especially for the synergistic effect with heat waves in summer, are not considered. These factors can influence physical mechanisms that drive the SUHIs and CUHIs, as well as the efficacy of heat mitigation strategies.[49,50] In-depth and extensive studies are required to elucidate the general principles.

STAR★METHODS

Detailed methods are provided in the online version of this paper and include the following:

- KEY RESOURCES TABLE
- RESOURCE AVAILABILITY
  - Lead contact
  - Materials availability
  - Data and code availability
- METHODS DETAILS
  - Urban morphology
  - Background climate
  - Mechanistic attribution model
  - UHI components

SUPPLEMENTAL INFORMATION

Supplemental information can be found online at https://doi.org/10.1016/j.isci.2024.108863.

ACKNOWLEDGMENTS

This research was supported by the National Natural Science Foundation of China (No. 51838011, No. 52078407, and No. 52178076). The weather data were kindly provided by China building energy efficiency design basic data platform (https://buildingdata.xauat.edu.cn/), EnergyPlus (https://energyplus.net/weather), and China Meteorological Data Network (http://data.cma.cn/). All the simulations were supported by the State Key Laboratory of Green Building.

AUTHOR CONTRIBUTIONS

Y.L. and L.Y. conceptualized the research and designed the research framework; Q.L., Qiong Li, and Y.L. developed the model, and Q.L. conducted the simulation studies; Q.L. and Y.L. performed the data analysis; L.Z. and Z.L. contributed ideas to the data analysis; Q.L. and Y.L. performed the model validation; Q.L. and Y.L. drafted the manuscript, with discussions and contributions from Qiong Li, L.Y., Z.L., and other co-authors.

DECLARATION OF INTERESTS

The authors declare no competing interests.

Received: August 16, 2023
Revised: November 28, 2023
Accepted: January 8, 2024
Published: January 11, 2024

REFERENCES

1. Oke, T.R., Mills, G., Christen, A., and Voogt, J.A. (2017). Urban Climates (Cambridge University Press).
2. Manoli, G., Fatichi, S., Schläpfer, M., Yu, K., Crowther, T.W., Meili, N., Burlando, P., Katul, G.G., and Bou-Zeid, E. (2019). Magnitude of urban heat islands largely explained by climate and population. Nature *573*, 55–60.
3. Jay, O., Capon, A., Berry, P., Broderick, C., de Dear, R., Havenith, G., Honda, Y., Kovats, R.S., Ma, W., Malik, A., et al. (2021). Reducing the health effects of hot weather and heat extremes: from personal cooling strategies to green cities. Lancet *398*, 709–724.
4. Ebi, K.L., Capon, A., Berry, P., Broderick, C., de Dear, R., Havenith, G., Honda, Y., Kovats, R.S., Ma, W., Malik, A., et al. (2021). Hot weather and heat extremes: health risks. Lancet *398*, 698–708.
5. Hajat, S., O'Connor, M., and Kosatsky, T. (2010). Health effects of hot weather: from awareness of risk factors to effective health protection. Lancet *375*, 856–863.
6. Su, M.A., Ngarambe, J., Santamouris, M., and Yun, G.Y. (2021). Empirical evidence on the impact of urban overheating on building cooling and heating energy consumption. iScience *24*, 102495.
7. Santamouris, M., Cartalis, C., Synnefa, A., and Kolokotsa, D. (2015). On the impact of urban heat island and global warming on the power demand and electricity consumption of buildings—A review. Energy Build. *98*, 119–124.
8. Sarrat, C., Lemonsu, A., Masson, V., and Guédalia, D. (2006). Impact of urban heat island on regional atmospheric pollution. Atmos. Environ. *40*, 1743–1758.
9. Fallmann, J., Forkel, R., and Emeis, S. (2016). Secondary effects of urban heat island mitigation measures on air quality. Atmos. Environ. *125*, 199–211.
10. Sabrin, S., Karimi, M., Fahad, M.G.R., and Nazari, R. (2020). Quantifying environmental and social vulnerability: Role of urban Heat Island and air quality, a case study of Camden, NJ. Urban Clim. *34*, 100699.
11. Rydin, Y., Bleahu, A., Davies, M., Dávila, J.D., Friel, S., De Grandis, G., Groce, N., Hallal, P.C., Hamilton, I., Howden-Chapman, P., et al. (2012). Shaping cities for health: complexity and the planning of urban environments in the 21st century. Lancet *379*, 2079–2108.
12. Haines, A., Kovats, R.S., Campbell-Lendrum, D., and Corvalán, C. (2006). Climate change and human health: impacts, vulnerability and public health. Public health *120*, 585–596.
13. Li, D., and Bou-Zeid, E. (2013). Synergistic interactions between urban heat islands and heat waves: The impact in cities is larger than the sum of its parts. J. Appl. Meteorol. Climatol. *52*, 2051–2064.
14. Habitat, U.N. (2022). World Cities Report 2022: Envisaging the Future of Cities.
15. Yang, J., Zhou, M., Ren, Z., Li, M., Wang, B., Liu, D.L., Ou, C.Q., Yin, P., Sun, J., Tong, S., et al. (2021). Projecting heat-related excess mortality under climate change scenarios in China. Nat. Commun. *12*, 1039.
16. Wang, J., Chen, Y., Liao, W., He, G., Tett, S.F.B., Yan, Z., Zhai, P., Feng, J., Ma, W., Huang, C., and Hu, Y. (2021). Anthropogenic emissions and urbanization increase risk of compound hot extremes in cities. Nat. Clim. Chang. *11*, 1084–1089.
17. Howard, L. (2012). The climate of London: deduced from meteorological observations (Cambridge University Press). https://www.cambridge.org/core/books/climate-of-london/E5796F1775785528A606DCFAD883E979.
18. Liu, Z., Cheng, K.Y., He, Y., Jim, C.Y., Brown, R.D., Shi, Y., Lau, K., and Ng, E. (2022). Microclimatic measurements in tropical cities: Systematic review and proposed guidelines. Build. Environ. *222*, 109411.
19. Stewart, I.D. (2011). A systematic review and scientific critique of methodology in modern urban heat island literature. Int. J. Climatol. *31*, 200–217.
20. Paschalis, A., Chakraborty, T.C., Fatichi, S., Meili, N., and Manoli, G. (2021). Urban forests as main regulator of the evaporative cooling effect in cities. AGU Advances *2*, e2020AV000303.
21. Venter, Z.S., Chakraborty, T., and Lee, X. (2021). Crowdsourced air temperatures contrast satellite measures of the urban heat island and its mechanisms. Sci. Adv. *7*, eabb9569.
22. Yang, J., Menenti, M., Wu, Z., Wong, M.S., Abbas, S., Xu, Y., and Shi, Q. (2021). Assessing the impact of urban geometry on surface urban heat island using complete and nadir temperatures. Int. J. Climatol. *41*, E3219–E3238.
23. Yang, J., Wong, M.S., Ho, H.C., Krayenhoff, E.S., Chan, P.W., Abbas, S., and Menenti, M. (2020). A semi-empirical method for estimating complete surface temperature from radiometric surface temperature, a study in Hong Kong city. Remote Sensing of Environment *237*, 111540.
24. Li, D., Liao, W., Rigden, A.J., Liu, X., Wang, D., Malyshev, S., and Shevliakova, E. (2019). Urban heat island: Aerodynamics or imperviousness? Sci. Adv. *5*, eaau4299.
25. Zhao, L., Lee, X., Smith, R.B., and Oleson, K. (2014). Strong contributions of local background climate to urban heat islands. Nature *511*, 216–219.
26. Manoli, G., Fatichi, S., Bou-Zeid, E., and Katul, G.G. (2020). Seasonal hysteresis of surface urban heat islands. Proc. Natl. Acad. Sci. USA *117*, 7082–7089.
27. Yang, C., Yan, F., and Zhang, S. (2020). Comparison of land surface and air temperatures for quantifying summer and winter urban heat island in a snow climate city. J. Environ. Manage. *265*, 110563.
28. Hu, Y., Hou, M., Jia, G., Zhao, C., Zhen, X., and Xu, Y. (2019). Comparison of surface and canopy urban heat islands within megacities of eastern China. ISPRS J. Photogrammetry Remote Sens. *156*, 160–168.
29. Zhang, Z., Paschalis, A., Mijic, A., Meili, N., Manoli, G., van Reeuwijk, M., and Fatichi, S. (2022). A mechanistic assessment of urban heat island intensities and drivers across climates. Urban Clim. *44*, 101215.
30. Ho, H.C., Knudby, A., Xu, Y., Hodul, M., and Aminipouri, M. (2016). A comparison of urban heat islands mapped using skin temperature, air temperature, and apparent temperature (Humidex), for the greater Vancouver area. Sci. Total Environ. *544*, 929–938.
31. Anderson, G.B., Bell, M.L., and Peng, R.D. (2013). Methods to calculate the heat index as an exposure metric in environmental health research. Environ. Health Perspect. *121*, 1111–1119.
32. Awasthi, A., Vishwakarma, K., and Pattnayak, K.C. (2022). Retrospection of heatwave and heat index. Theor. Appl. Climatol. *147*, 589–604.
33. Ali-Toudert, F. (2021). Exploration of the thermal behaviour and energy balance of urban canyons in relation to their geometrical and constructive properties. Build. Environ. *188*, 107466.
34. Schulze, H., and Langenberg, H. (2014). Urban heat. Nat. Geosci. *7*, 553.
35. Yu, Z., Xu, S., Zhang, Y., Jørgensen, G., and Vejre, H. (2018). Strong contributions of local background climate to the cooling effect of urban green vegetation. Sci. Rep. *8*, 6798–6799.
36. Shashua-Bar, L., Pearlmutter, D., and Erell, E. (2009). The cooling efficiency of urban landscape strategies in a hot dry climate. Landsc. Urban Plann. *92*, 179–186.
37. Allen, L., Lindberg, F., and Grimmond, C.S.B. (2011). Global to city scale urban anthropogenic heat flux: model and variability. Int. J. Climatol. *31*, 1990–2005.
38. Adelia, A.S., Yuan, C., Liu, L., and Shan, R.Q. (2019). Effects of urban morphology on anthropogenic heat dispersion in tropical high-density residential areas. Energy Build. *186*, 368–383.
39. Besir, A.B., and Cuce, E. (2018). Green roofs and facades: A comprehensive review. Renew. Sustain. Energy Rev. *82*, 915–939.
40. Wong, N.H., Tan, C.L., Kolokotsa, D.D., and Takebayashi, H. (2021). Greenery as a mitigation and adaptation strategy to urban heat. Nat. Rev. Earth Environ. *2*, 166–181.
41. Shastri, H., Barik, B., Ghosh, S., Venkataraman, C., and Sadavarte, P. (2017). Flip flop of day-night and summer-winter surface urban heat island intensity in India. Sci. Rep. *7*, 40178.
42. Spronken-Smith, R.A., and Oke, T.R. (1998). The thermal regime of urban parks in two cities with different summer climates. Int. J. Rem. Sens. *19*, 2085–2104.
43. Cuthbert, M.O., Rau, G.C., Ekström, M., O'Carroll, D.M., and Bates, A.J. (2022). Global climate-driven trade-offs between the water retention and cooling benefits of urban greening. Nat. Commun. *13*, 518.
44. Ziter, C.D., Pedersen, E.J., Kucharik, C.J., and Turner, M.G. (2019). Scale-dependent interactions between tree canopy cover and impervious surfaces reduce daytime urban heat during summer. Proc. Natl. Acad. Sci. USA *116*, 7575–7580.
45. Gunawardena, K.R., Wells, M.J., and Kershaw, T. (2017). Utilising green and bluespace to mitigate urban heat island intensity. Sci. Total Environ. *584–585*, 1040–1055.
46. Zhang, K., Cao, C., Chu, H., Zhao, L., Zhao, J., and Lee, X. (2023). Increased heat risk in wet climate induced by urban humid heat. Nature *617*, 738–742.
47. Schwaab, J., Meier, R., Mussetti, G., Seneviratne, S., Bürgi, C., and Davin, E.L. (2021). The role of urban trees in reducing land surface temperatures in European cities. Nat. Commun. *12*, 6763.
48. Gober, P., Brazel, A., Quay, R., Myint, S., Grossman-Clarke, S., Miller, A., and Rossi, S. (2009). Using watered landscapes to manipulate urban heat island effects: how much water will it take to cool Phoenix? J. Am. Plann. Assoc. *76*, 109–121.

49. Xue, J., Zong, L., Yang, Y., Bi, X., Zhang, Y., and Zhao, M. (2023). Diurnal and interannual variations of canopy urban heat island (CUHI) effects over a mountain–valley city with a semi-arid climate. Urban Clim. *48*, 101425.
50. Yang, Y., Guo, M., Wang, L., Zong, L., Liu, D., Zhang, W., Wang, M., Wan, B., and Guo, Y. (2023). Unevenly spatiotemporal distribution of urban excess warming in coastal Shanghai megacity, China: Roles of geophysical environment, ventilation and sea breezes. Build. Environ. *235*, 110180.
51. Li, H., Liu, Y., Zhang, H., Xue, B., and Li, W. (2021). Urban morphology in China: Dataset development and spatial pattern characterization. Sustain. Cities Soc. *71*, 102981.
52. Liu, Y., Li, Q., Yang, L., Mu, K., Zhang, M., and Liu, J. (2020). Urban heat island effects of various urban morphologies under regional climate conditions. Sci. Total Environ. *743*, 140589.
53. Yang, C., and Zhao, S. (2022). A building height dataset across China in 2017 estimated by the spatially-informed approach. Sci. Data *9*, 76.
54. Li, H., Yuan, F., Shen, L., Liu, Y., Zheng, Z., and Zhou, X. (2022). Improving the WRF/urban modeling system in China by developing a national urban dataset. Geosci. Front. *13*, 101385.
55. Brutsaert, W. (1975). On a derivable formula for long-wave radiation from clear skies. Water Resour. Res. *11*, 742–744.
56. Dingman, S.L. (2015). Physical Hydrology (Waveland press).
57. Zeng, Z., Piao, S., Li, L.Z.X., Zhou, L., Ciais, P., Wang, T., Li, Y., Lian, X., Wood, E.F., Friedlingstein, P., et al. (2017). Climate mitigation from vegetation biophysical feedbacks during the past three decades. Nat. Clim. Chang. *7*, 432–436.
58. Li, D., Malyshev, S., and Shevliakova, E. (2016). Exploring historical and future urban climate in the Earth System Modeling framework: 1. Model development and evaluation. J. Adv. Model. Earth Syst. *8*, 917–935.
59. Kikegawa, Y., Genchi, Y., Yoshikado, H., and Kondo, H. (2003). Development of a numerical simulation system toward comprehensive assessments of urban warming countermeasures including their impacts upon the urban buildings' energy-demands. Appl. Energy *76*, 449–466.
60. Sailor, D.J., and Fan, H. (2004). The importance of including anthropogenic heating in mesoscale modeling of the urban heat island. Bull. Am. Meteorol. Soc. 397–403.
61. Oke, T.R. (2002). Boundary Layer Climates (Routledge).
62. Harman, I.N., Best, M.J., and Belcher, S.E. (2004). Radiative exchange in an urban street canyon. Boundary-Layer Meteorol. *110*, 301–316.
63. Bueno, B., Norford, L., Hidalgo, J., and Pigeon, G. (2013). The urban weather generator. Journal of Building Performance Simulation *6*, 269–281.
64. Yang, J., Wong, M.S., Menenti, M., Nichol, J., Voogt, J., Krayenhoff, E.S., and Chan, P.W. (2016). Development of an improved urban emissivity model based on sky view factor for retrieving effective emissivity and surface temperature over urban areas. ISPRS J. Photogrammetry Remote Sens. *122*, 30–40.
65. Sobrino, J.A., Oltra-Carrió, R., Jiménez-Muñoz, J., Julien, Y., Sòria, G., Franch, B., and Mattar, C. (2012). Emissivity mapping over urban areas using a classification-based approach: Application to the Dual-use European Security IR Experiment (DESIREX). Int. J. Appl. Earth Obs. Geoinf. *18*, 141–147.
66. Chen, L., Ng, E., An, X., Ren, C., Lee, M., Wang, U., and He, Z. (2012). Sky view factor analysis of street canyons and its implications for daytime intra-urban air temperature differentials in high-rise, high-density urban areas of Hong Kong: a GIS-based simulation approach. Int. J. Climatol. *32*, 121–136.
67. Macdonald, R.W., Griffiths, R.F., and Hall, D.J. (1998). An improved method for the estimation of surface roughness of obstacle arrays. Atmos. Environ. *32*, 1857–1864.
68. Grimmond, C.S.B., and Oke, T.R. (1999). Heat storage in urban areas: Local-scale observations and evaluation of a simple model. J. Appl. Meteor. *38*, 922–940.
69. Meyn, S.K., and Oke, T.R. (2009). Heat fluxes through roofs and their relevance to estimates of urban heat storage. Energy Build. *41*, 745–752.

STAR★METHODS

KEY RESOURCES TABLE

REAGENT or RESOURCE	SOURCE	IDENTIFIER
Background meteorological data		
Typical meteorological year data	China building energy efficiency design basic data platform	https://buildingdata.xauat.edu.cn/
	EnergyPlus	https://energyplus.net/weather
Mean annual precipitation data	China Meteorological Data Network	http://data.cma.cn/

RESOURCE AVAILABILITY

Lead contact

Requests for further information and resources should be directed to the lead contact, Liu Yan (liuyan@xauat.edu.cn).

Materials availability

This study did not generate new materials.

Data and code availability

All data can be obtained from the lead contact, provided the request is reasonable.

The code related to the attribution model can be accessed by reaching out to the lead contact.

METHODS DETAILS

Urban morphology

The present study focused on the thermal environment in residential areas at the neighborhood scale ($\leq$ 1 km). It is generally assumed that megacities contain more tall buildings but according to a recent study of 36 major cities in China, the mean building height at the city level is not related to the city size, and the urban morphology parameters (building height, building width, and street width) are similar in residential areas.[51] At the neighborhood scale, various urban morphologies are present in Chinese cities, and urban morphology also has a significant impact on the urban thermal environment.[52] Therefore, when analyzing the impact of background climatic conditions on UHIs, the influence generated by changes in urban morphology was eliminated by selecting the common urban morphology as the base case for the model. Additionally, the impact of urban morphology on UHIs has also been studied, we selected combinations of different urban morphology parameters. According to the building height data set for China, the average building height is generally below 20 m.[51,53] Beijing City Lab (https://www.beijingcitylab.com/) provides data for 141375 street blocks in 63 Chinese cities during 2017, with three-dimensional parameters at the street block scale for these Chinese cities. According to this data set, the average number of building stories is predominantly <7 in China, which is also consistent with the results obtained in a previous study,[51,53] and the building density is mainly medium and high density (ρ_b > 0.25) in these street blocks. Therefore, the urban morphology parameters established for the base case in the study comprised: building height h_b = 18 m (about 6 stories), building density ρ_b = 0.3, building width w_b = 20 m,[54] and $g_{c,u}$ = 0.3. We also considered the effects of differences in urban morphology by changing the building density, in the range of 0.2–0.6, based on the street block data from 63 Chinese cities provided by the Beijing City Lab, which shows most building densities in China ranged from 0.22 to 0.52.

Background climate

The climate conditions vary significantly among years and the background climate data for a given year do not reflect the general UHIs in a city. Thus, it is required a customized background climate data set that adequately reflected the typical background climatic conditions in cities, so we obtained typical meteorological year data from the China building energy efficiency design basic data platform (https://buildingdata.xauat.edu.cn/) as background meteorological data. Typical meteorological year data for Macau and Taipei were obtained from EnergyPlus (https://energyplus.net/weather). Mean annual precipitation data were retrieved from the 1970–2017 monthly precipitation data set of the China Meteorological Data Network (http://data.cma.cn/).

Mathematical model

Multivariable functions of T_s (surface temperature) and T_c (air temperature) were derived from the energy balance in rural or urban areas. Next, based on the first-order Taylor series expansion, the mechanistic attribution model for attributing the UHI intensity to contributions from different factors was developed (radiation, evapotranspiration, convection efficiency, heat storage, and anthropogenic heat).[2,24,25] The

surface energy balance model validation was performed with the 2013 Global Urban Heat Island Dataset, which was provided by Manoli et al.[2] We selected cities with populations over 10^5 for model validation. The observed urban surface temperature was obtained from the observed rural surface temperature + urban heat island intensity (i.e. Ts_summer_2013 + dTs_summer_2013). Comparison of the surface temperature observed and simulated in rural and urban areas were shown in Figures S12A and S12B, respectively. The surface energy balance model shows higher accuracy in rural areas (rural: RMSE = 1.0°C, urban: RMSE = 4.3°C), due to the more complex urban underlying surface in urban areas. The canopy energy balance model validation was performed with the observed data in Xi'an, China, in 2016, which available from China building energy efficiency design basic data platform (https://buildingdata.xauat.edu.cn/). The hourly meteorological data are averaged to obtain daily data for the model inputs. Comparison of the canopy air temperature observed and simulated in rural and urban areas were shown in Figures S13A and S13B, respectively. Similar to the surface energy balance model, the canopy energy balance model shows higher accuracy in rural areas (rural: RMSE = 0.1°C, urban: RMSE = 1.0°C). Considering the error caused by the first-order Taylor series expansion of the mechanistic attribution model, the mean values of the rural and urban variables were used as parameters in this model, the mechanistic attribution model validation as shown in Figures S12C and S13C.

Mechanistic attribution model

Based on the first-order Taylor series expansion, we attributed the UHI intensity (including SUHIs and CUHIs) to contributions from different biophysical factors. For SUHIs, based on the surface energy balance equation:

$$Q^* = S^* + L^* = Q_H + Q_E + Q_G \quad \text{(Equation 1)}$$

where Q^* is the net surface radiation [$W \cdot m^{-2}$], S^* is the net short-wave radiation [$W \cdot m^{-2}$], i.e., $S^* = S_{in}(1 - \alpha)$, S_{in} is the incoming short-wave radiation [$W \cdot m^{-2}$], α is the surface albedo, and L^* is the net long-wave radiation [$W \cdot m^{-2}$], i.e., $L^* = L_{in} - L_{out}$, where L_{in} is the incoming long-wave radiation [$W \cdot m^{-2}$]. Considering that these data were missing for many areas, we modeled $L_{in} = \varepsilon_a \sigma T_a^4$[55], where ε_a is the atmospheric emissivity, i.e., $\varepsilon_a = 1.723\left(\frac{e_{sat}(T_a)\frac{RH}{100}}{T_a}\right)^{\frac{1}{7}}$, $e_{sat}(T_a)$ is the saturation vapor pressure at temperature T_a [kPa], i.e., $e_{sat}(T_a) = 0.611 \exp\left(\frac{17.27(T_a - 273.15)}{T_a - 35.85}\right)$[56], σ is the Stefan–Boltzmann constant ($\sigma = 5.67 \times 10^{-8}\ W \cdot m^{-2} \cdot K^{-4}$), and T_a is the air temperature which measurement at the rural weather station [K]. In addition, L_{out} is the upward long-wave radiation [$W \cdot m^{-2}$], i.e., $L_{out} = \varepsilon_s \sigma T_s^4 + (1 - \varepsilon_s) L_{in}$, where ε_s is the surface emissivity and T_s is the LST [K]. Q_H is the sensible heat flux [$W \cdot m^{-2}$], i.e., $Q_H = \frac{\rho c_p (T_s - T_a)}{r_a}$, where ρ is the air density [$kg \cdot m^{-3}$], c_p is the specific heat of air at constant pressure [$J \cdot kg^{-1} \cdot K^{-1}$], and r_a is the aerodynamic resistance [$s \cdot m^{-1}$]. Q_E is the latent heat flux [$W \cdot m^{-2}$], i.e., $Q_E = g_c \beta \frac{\rho l_v [q_{sat}(T_s) - q_a]}{r_a + r_s}$, where g_c is the green cover, β is the water stress factor, l_v is the latent heat of vaporization [$J \cdot kg^{-1}$], and $q_{sat}(T_s)$ is the saturated specific humidity at temperature T_s [$kg \cdot kg^{-1}$], i.e., $q_{sat}(T_s) = 0.622 \frac{esat(Ts)}{patm - 0.378esat(Ts)}$, where p_{atm} is the atmospheric pressure [kPa], q_a is the specific humidity of air [$kg \cdot kg^{-1}$], and r_s is the surface resistance [$s \cdot m^{-1}$]. Q_G is the heat storage [$W \cdot m^{-2}$], which can be modeled by the objective hysteresis model (OHM). In this surface energy balance equation, we considered the heat exchange between the urban surface and the atmosphere (Q_H), while excluding the impact of urban canopy air temperature. Subsequently, we obtain the surface temperature as a boundary condition for the canopy energy balance equation (Q_s). Meanwhile, the anthropogenic heat flux directly affects air in the urban canopy to increase the air temperature, which then indirectly affects the heat dissipation from the urban surface, so we considered the effect of anthropogenic heat flux in the canopy energy balance equation (see the next section).

To obtain an analytical form of T_s, the outgoing long-wave radiation term and the saturated specific humidity term were linearized at the point T_a:

$$\varepsilon_s \sigma T_s^4 \approx \varepsilon_s \sigma T_a^4 + 4\varepsilon_s \sigma T_a^3 (T_s - T_a) \quad \text{(Equation 2)}$$

$$q_{sat}(T_s) \approx q_{sat}(T_a) + q'_{sat,s}(T_a)(T_s - T_a) \quad \text{(Equation 3)}$$

where $q'_{sat,s}(T_a)$ is the derivative of $q_{sat}(T_a)$ relative to T_a.

By substituting Equations 2 and 3 into Equation 1 and rearranging, built the following analytical solution for T_s.

$$T_s = \frac{S_{in}(1 - \alpha) + \varepsilon_s \sigma (\varepsilon_a - 1) T_a^4 - g_c \beta \frac{\rho l_v [q_{sat}(T_a) - q_a]}{r_a + r_s} - Q_G}{4\varepsilon_s \sigma T_a^3 + \frac{\rho c_p}{r_a} + g_c \beta \frac{\rho l_v}{r_a + r_s} q'_{sat}(T_a)} + T_a \quad \text{(Equation 4)}$$

In this study, urbanization was considered as a perturbation of the rural base state and only consider changes in LST due to changes in five biophysical factors (i.e., $\Delta\alpha$, $\Delta\varepsilon_s$, Δr_a, Δr_s, and ΔQ_G). According to Taylor's theorem, the urban–rural LST difference was expressed as:

$$\Delta T_s = \frac{1}{f_s}\left\{\begin{array}{l} -S_{in}\Delta\alpha + \sigma\left(\varepsilon_a T_a^{\,4} - T_s^{\,4}\right)\Delta\varepsilon_s + \left[\frac{\rho c_p}{r_a^{\,2}}\left(T_s - T_a\right) + g_c\beta\frac{\rho l v\left[q_{sat}(T_s) - q_a\right]}{\left(r_a+r_s\right)^2}\right]\Delta r_a \\ +\beta\frac{\rho l v\left[q_{sat}(T_s) - q_a\right]}{r_a+r_s}\Delta g_c - \Delta Q_G \end{array}\right\} \quad \text{(Equation 5)}$$

$$f_s = 4\varepsilon_s\sigma T_s^{\,3} + \frac{\rho c_p}{r_a} + g_c\beta\frac{\rho l_v}{r_a+r_s}q'_{sat}(T_s) \quad \text{(Equation 6)}$$

where f_s^{-1} represents the sensitivity of LST to changes of 1 $W\cdot m^{-2}$ in energy forcing at the land surface.[2,57]

Similar to SUHI, CUHI is based on the canopy energy balance equation:

$$Q_c = Q_s + Q_{ah} \quad \text{(Equation 7)}$$

where Q_c denotes turbulent exchanges between the air temperature in the urban canyon and atmosphere [$W\cdot m^{-2}$], i.e., $Q_c = \frac{\rho c_p(T_c - T_{atm})}{r_a}$[58]; T_{atm} is the temperature of the atmosphere above the urban canopy [K], and considering that these data were missing for many cities, which was assumed that it was equal to the air temperature measured at the rural weather station, i.e., $T_{atm} = T_a$; T_c is the canopy air temperature [K], Q_s denotes turbulent exchanges between the air temperature in the urban canyon and urban surface [$W\cdot m^{-2}$], i.e., $Q_s = \rho c_p C_h(T_s - T_c)$, C_h denotes the turbulent transfer coefficient for sensible heat [$s\cdot m^{-1}$], and Q_{ah} is the anthropogenic heat flux [$W\cdot m^{-2}$] calculated based on the building energy model framework.[59] In residential buildings, the heat load generated by indoor human metabolism and heat dissipation from equipment (electric lights, etc.) is relatively small relative to the overall anthropogenic heat, so only considered the heat load generated by heat transfer through the building structure and ventilation into the room[60]: $Q_{ah} = (H_{out} + E_{out})\frac{1+COP}{COP}$, where H_{out} and E_{out} are the sensible and latent heat pumped out from the building, respectively, and COP represents the energy efficiency of heat source equipment. $H_{out} = [h(T_s - T_{in}) + (1 - \beta_{in})\rho c_p v_a(T_c - T_{in})]\varphi_p$, where h is the convective heat transfer coefficient [$W\cdot m^{-2}\cdot K^{-1}$], T_{in} is the indoor air temperature [K], which was selected according to the local air temperature, β_{in} is the thermal efficiency of the total heat exchanger, v_a is the total ventilation rate in the building [$m^3\cdot h^{-1}$], and φ_p is the ratio of hourly occupants relative to the peak number of occupants per floor area ($0 \le \varphi_p \le 1$). $E_{out} = (1 - \beta_{in})l_v\rho v_a(q_a - q_{in})\varphi_p$, where q_{in} is the specific humidity of the indoor air [$kg\cdot kg^{-1}$].

By rearranging the canopy energy balance equation, built the following analytical solution for T_c.

$$T_c = \frac{\frac{\rho c_p T_{atm}}{r_a} + \rho c_p C_h T_s + Q_{ah}}{\frac{\rho c_p}{r_a} + \rho c_p C_h} \quad \text{(Equation 8)}$$

Similar to SUHI, according to Taylor's theorem, the urban–rural air temperature difference was expressed as:

$$\Delta T_c = \frac{1}{f_c}\left[\rho c_p C_h\Delta T_s + \frac{\rho c_p}{r_a^2}(T_c - T_{atm})\Delta r_a + \rho c_p(T_s - T_c)\Delta C_h + \Delta Q_{ah}\right] \quad \text{(Equation 9)}$$

$$f_c = \frac{\rho c_p}{r_a} + \rho c_p C_h \quad \text{(Equation 10)}$$

where f_c^{-1} represents the sensitivity of the air temperature to changes of 1 $W\cdot m^{-2}$ in energy forcing in the urban canyon.

The contributions to ΔT from different biophysical factors comprising R^*, ET, CV, G, and AH were expressed as:

$$Contribution_i = \frac{\Delta i|\Delta i|}{(\Delta R^*)^2 + (\Delta ET)^2 + (\Delta CV)^2 + (\Delta G)^2 + (\Delta AH)^2} \times 100\% \quad \text{(Equation 11)}$$

where $Contribution_i$ denotes the contribution of a particular biophysical factor, $i = \{R^*, ET, CV, G, AH\}$.

$$\Delta R^* = \left\{\begin{array}{ll} \frac{1}{f_s}\left(-S_{in}\Delta\alpha + \sigma\left(\varepsilon_a T_a^{\,4} - T_s^{\,4}\right)\Delta\varepsilon_s\right) & \text{in } \Delta T_s \\ \frac{1}{f_s}\frac{1}{f_c}\rho c_p C_h\left(-S_{in}\Delta\alpha + \sigma\left(\varepsilon_a T_a^{\,4} - T_s^{\,4}\right)\Delta\varepsilon_s\right) & \text{in } \Delta T_c \end{array}\right. \quad \text{(Equation 12)}$$

$$\Delta ET = \begin{cases} \frac{1}{f_s}\left(\beta\frac{\rho l_v\left[q_{sat}(T_s) - q_a\right]}{r_a+r_s}\Delta g_c\right) & \text{in } \Delta T_s \\ \frac{1}{f_s}\frac{1}{f_c}\rho c_p C_h\left(\beta\frac{\rho l_v\left[q_{sat}(T_s) - q_a\right]}{r_a+r_s}\Delta g_c\right) & \text{in } \Delta T_c \end{cases} \quad \text{(Equation 13)}$$

$$\Delta CV = \begin{cases} \frac{1}{f_s}\left(\left[\frac{\rho c_p}{r_a^2}(T_s - T_a) + g_c\beta\frac{\rho lv\left[q_{sat}(T_s) - q_a\right]}{(r_a+r_s)^2}\right]\Delta r_a\right) & \text{in } \Delta T_s \\ \frac{1}{f_s}\frac{1}{f_c}\rho c_p C_h\left(\beta\frac{\rho l_v\left[q_{sat}(T_s) - q_a\right]}{r_a+r_s}\Delta g_c\right) + \frac{1}{f_c}\left(\frac{\rho c_p}{r_a^2}(T_c - T_{atm})\Delta r_a + \rho c_p(T_s - T_c)\Delta C_h\right) & \text{in } \Delta T_c \end{cases} \quad \text{(Equation 14)}$$

$$\Delta G = \begin{cases} \frac{1}{f_s}(-\Delta Q_G) & \text{in } \Delta T_s \\ \frac{1}{f_s}\frac{1}{f_c}\rho c_p C_h(-\Delta Q_G) & \text{in } \Delta T_c \end{cases} \quad \text{(Equation 15)}$$

$$\Delta AH = \frac{1}{f_c}(\Delta Q_{ah}) \quad \text{in } \Delta T_c \quad \text{(Equation 16)}$$

UHI components

Albedo, α

The urban surface albedo (α_{urban}) is influenced by the reflective properties of urban surface materials and the urban geometry (cavity effect).[61] Considering the radiation exchange process in the urban canopy, the derived α_{urban} is more accurate when the reflection is calculated in the urban canopy more times. Numerical simulation studies have shown that it is sufficient to consider only two reflection processes in practice.[62] The α_{urban} was calculated by considering two reflection processes:

$$\alpha_{urban} = \frac{2h_b\left(\begin{matrix}\alpha_w SVF_w+\alpha_w{}^2 SVF_{ww}SVF_w \\ +\alpha_w\alpha_r SVF_{rw}SVF_r\end{matrix}\right)+w_r(\alpha_r SVF_r+2\alpha_r\alpha_w SVF_{wr}SVF_w)}{2h_b+w_r} \quad \text{(Equation 17)}$$

where h_b is the building height [m], w_r is the road width [m], α_w is the albedo of the wall, α_r is the albedo of the road, and *SVF* denotes the sky view factors calculated as: $SVF_w = \frac{1}{2}\left(h_b/_{w_r} + 1 - \sqrt{\left(h_b/_{w_r}\right)^2+1}\right)\div\left(h_b/_{w_r}\right) = SVF_{rw}$, $SVF_r = \sqrt{\left(h_b/_{w_r}\right)^2+1} - h_b/_{w_r}$, $SVF_{ww} = 1 - 2SVF_w$, $SVF_{wr} = \frac{1}{2}(1 - SVF_r)$.[63]

The rural surface albedo (α_{rural}) was selected based on the typical surface albedo values provided by the local climate zone (LCZ) system. The change in albedo induced by urbanization was calculated as follows.

$$\Delta\alpha = \alpha_{urban} - \alpha_{rural} \quad \text{(Equation 18)}$$

Emissivity, ε

Considering the "trapping" effect of urban geometry on long-wave radiation (cavity effect), the effective emissivity of the urban canopy was calculated as[64]:

$$\varepsilon_{urban} = \frac{\varepsilon_{u,0}}{1 - (1 - \varepsilon_{u,0})(1 - SVF)} \quad \text{(Equation 19)}$$

where $\varepsilon_{u,0}$ is the emissivity of the urban fabric (assumed to be 0.9[65]) and *SVF* is the sky view factor of the urban canopy, i.e., $SVF = \left\{\cos\left[\arctan\left(\frac{H}{W}\right)\right]\right\}^2$.[66]

Satellite observations show that the emissivity varies little over mostly vegetated surfaces and it deviates only slightly from 0.95 among different land cover types.[57] Therefore, for vegetation-covered suburban areas, assumed a surface emissivity of: $\varepsilon_{rural} = 0.95$.

The change in emissivity induced by urbanization was calculated as follows.

$$\Delta\varepsilon = \varepsilon_{urban} - \varepsilon_{rural} \quad \text{(Equation 20)}$$

Aerodynamic resistance, r_a

The aerodynamic resistance (r_a) was used to represent the degree to which atmospheric turbulence facilitates the transport of heat from a surface. Based on Monin–Obukhov similarity theory, the r_a values for urban ($r_{a,urban}$) and rural ($r_{a,rural}$) areas can be modeled as:

$$r_a = \frac{\ln\left(\frac{z_m - d}{z_{0,m}}\right)\ln\left(\frac{z_m - d}{z_{0,h}}\right)}{k_v^2 u(z)} \quad \text{(Equation 21)}$$

where k_v is the von Karman's constant, $k_v = 0.41$, $u(z)$ is the wind speed [$m \cdot s^{-1}$], z_m is the height of wind measurements [m], we assume that the urban effect on wind speed can be neglected at $z_m = 2.5h_b$, $u(z)$ be assumed equal in urban and rural areas and calculated with the 10m wind speed at the rural weather station, d is the zero plane displacement height [m], which was calculated in urban (d_u) and rural (d_r) areas as[67]: $d_u = [1 + m_\alpha^{-\lambda_p}(\lambda_p - 1)]h_b$, $d_r = 0.67h_v$, where m_α (= 4) is an empirical constant, λ_p is the plant area density, and h_b and h_v are the building and vegetation canopy heights, respectively, i.e., $h_v = \frac{22.47}{1+\exp[-0.0046(P-445.17)]}^2$, where P is the mean annual precipitation [$mm \cdot yr^{-1}$], $z_{0,m}$ and $z_{0,h}$ are the roughness lengths for momentum and heat transfer, respectively [m], which were calculated for urban ($z_{0,mu}$) and rural ($z_{0,mr}$) areas as: $z_{0,mu} = \left(1 - \frac{d_u}{h_b}\right)\exp\left\{-\left[0.5\frac{C_d}{k_v^2}\left(1 - \frac{d_u}{h_b}\right)\lambda_f\right]^{-0.5}\right\}h_b$, $z_{0,mr} = 0.123h_v$, where C_d (= 1.2) is an empirical constant, λ_f is the frontal area density, i.e., $\lambda_f = \frac{VH_{urb}}{4}$, and VH_{urb} is the vertical-to-horizontal urban area ratio; and $z_{0,h}$ is usually calculated by $z_{0,h} = 0.1z_{0,m}$, although the aerodynamic resistances to heat and momentum transfer are not necessarily monotonically or linearly related, but this simple relationship was adequate for application in this study.[2]

The change in emissivity induced by urbanization was calculated as follows.

$$\Delta r_a = r_{a,urban} - r_{a,rural} \quad \text{(Equation 22)}$$

Green cover (g_c) and evapotranspiration

In this study, the effect of difference in urban green cover ($g_{c,u}$) on UHIs was considered, where $g_{c,u} = 0.3$ was used as the base case. It was assumed that rural areas are adequately covered by vegetation ($g_{c,r} = 1$). The actual evapotranspiration is controlled by energy and water availability. The water stress factor was used to describe water limitation, $\beta = 1 + \frac{P}{PET} - \left[1 - I_r + \left(\frac{P}{PET}\right)^{\omega}\right]^{1/\omega}$[2], where ω (=2.1) is a model parameter, I_r ($0 \le I_r \le 1$) represents the level of irrigation, and PET is the potential evapotranspiration [$mm \cdot yr^{-1}$], i.e., $PET = \rho\frac{q_{sat}(T_s) - q_a}{r_a + r_s}\frac{\eta}{\rho_w}$, where η is a unit conversion factor and ρ_w is the density of water [$kg \cdot m^{-3}$].

Heat storage, Q_G

The OHM was used to parameterize the heat storage (Q_G)[68]:

$$Q_G = \sum_{i=1}^{n}(f_i a_{1i})Q^* + \sum_{i=1}^{n}(f_i a_{2i})\left(\frac{\partial Q^*}{\partial t}\right) + \sum_{i=1}^{n}(f_i a_{3i}) \quad \text{(Equation 23)}$$

where i are different surface types, f_i is the surface fraction occupied by each of the i types, and the coefficients a_1, a_2, and a_3 were derived from independent empirical studies,[68,69] where a_1 considers the strength of the mean dependence of Q_G on the net surface radiation Q^* [-], a_2 considers the degree and direction of the phase relationships between Q_G and Q^* [h], and a_3 is the intercept term [$W \cdot m^{-2}$].